

Interacting dark sector with quadratic coupling: theoretical and observational viability

Jaelsson S. Lima^{a1}, Rodrigo von Marttens^{b2,3}, and Luciano Casarini^{c1}

¹ Departamento de Física, Universidade Federal de Sergipe, São Cristóvão, SE, 49107-230, Brazil

² Instituto de Física, Universidade Federal da Bahia, Salvador, BA, 40170-155, Brazil

³ PPGCosmo, Universidade Federal do Espírito Santo, Vitória, ES, 29075-910, Brazil

Received: date / Revised version: date

Abstract. Models proposing a non-gravitational interaction between dark energy (DE) and dark matter (CDM) have been extensively studied as alternatives to the standard cosmological model. A common approach to describing the DE-CDM coupling assumes it to be linearly proportional to the dark energy density. In this work, we consider the model with interaction term $Q = 3H\gamma\rho_x^2/(\rho_c + \rho_x)$. We show that for positive values of γ this model predicts a future violation of the Weak Energy Condition (WEC) for the dark matter component, and for a specific range of negative values of γ the CDM energy density can be negative in the past. We perform a parameter selection analysis for this model using data from Type Ia supernovae, Cosmic Chronometers, Baryon Acoustic Oscillations, and CMB combined with the Hubble constant H_0 prior. Imposing a prior to ensure that the WEC is not violated, our model is consistent with Λ CDM in 2σ C.L.. In reality, the WEC prior shifts the constraints towards smaller values of H_0 , highlighting an increase in the tension on the Hubble parameter. However, it significantly improves the parameter constraints, with a preference for smaller values of σ_8 , alleviating the σ_8 tension between the CMB results from Planck 2018 and the weak gravitational lensing observations from the KiDS-1000 cosmic shear survey. In the case without the WEC prior, our model seems to alleviate the H_0 tension, which is related to the positive value of the interaction parameter γ .

Key words. Cosmology – Dark energy – Dark matter – Interacting model – Cosmological parameters

PACS. XX.XX.XX No PACS code given

1 Introduction

In the face of the discovery of the accelerated expansion of the Universe from observations of Type Ia Supernovae (SNe Ia) [1, 2, 3], a new model of the Universe comes into effect, containing characteristics of negative pressure energy content, referred to in the literature as dark energy (DE) [4]. Despite the great observational success of the standard Λ CDM model, where CDM stands for cold dark matter, it presents some shortcomings, such as the cosmological constant problem, the cosmic coincidence, and the Hubble constant tension. Therefore several models or approaches are attempting to obtain a better description of the nature of dark energy, which could be theoretically associated with quantum vacuum states. However, the cosmological constant still stands as the simplest candidate

to be the component of dark energy [5, 6, 7, 8, 9, 10, 11, 12, 13, 14, 15].

In this work, we focus on a class of interacting models commonly referred to in the literature as interacting dark energy models (IDEM), with particular attention to the model designated as IDEM 2 in Ref. [10]. These models depart from the standard assumption of dark matter (DM) and dark energy (DE) as independent components by introducing a non-gravitational interaction, resulting in an energy exchange between them. Such interacting models are primarily phenomenologically motivated, reflecting our limited understanding of the fundamental physics underlying a coupling term [10, 16, 17].

A common choice for a IDEM assume that the interaction term Q is linearly proportional to the DE density, i.e., $Q = 3\gamma H\rho_x$, where H and γ represent the Hubble and interaction parameters, respectively (see, e.g., Refs. [10, 18, 19, 20, 21]). However, as demonstrated in Ref. [16], this class of models can exhibit non-physical behavior for certain parameter ranges, specifically predicting negative pressureless matter densities, thereby violating the Weak Energy Condition (WEC). In this work, we consider a model

^a e-mail: jaelsson.slima@gmail.com (corresponding author)

^b e-mail: rodrigoonmarttens@gmail.com

^c e-mail: lcasarini@academico.ufs.br

in which the interaction term is given by $Q \propto \rho_x^2 / (\rho_c + \rho_x)$, and deviating from the conventional linear interaction forms. The quadratic dependence on ρ_x introduces a richer dynamical evolution, reflecting a more complex interplay between DE and CDM. Nevertheless, similar to the linear case, we show that this model also presents non-physical behavior for specific parameter values, with implications for the Universe's background evolution and the growth of cosmic structures [22,23].

This paper is organized as follows: In Section 2, we introduce the background dynamics for the cosmological model in analysis. In Section 3, we present the linear perturbation theory for interacting perfect fluids, while in Section 4 we detail the observational data used, the methodology, and the statistical analysis involved. The statistical analysis is based on MontePython¹ and a suitable modified version of Cosmic Linear Anisotropy Solving System (CLASS)² codes. In Section 5, we discuss the main results obtained. Finally, we present our conclusions in Section 6.

2 Background Dynamics

Let's consider the energy balance equations, without fixing the state equation parameter at $\omega_x = -1$, but leaving it as a constant parameter. Thus, the energy conservation law for baryons, CDM, and DE are given, respectively, by

$$\dot{\rho}_b + 3H\rho_b = 0, \quad (1)$$

$$\dot{\rho}_c + 3H\rho_c = -Q, \quad (2)$$

$$\dot{\rho}_x + 3H\rho_x(1 + \omega_x) = Q, \quad (3)$$

where ρ_c , ρ_x , and ρ_b are respectively the densities of CDM, DE, and conserved baryons. The term ω_x is the DE equation-of-state (EoS) parameter. In this work, we are interested in the energy exchange between DM and DE described by the IDEM 2 in Ref. [10], which is characterized by the interaction term given by

$$Q = 3H\gamma \frac{\rho_x^2}{\rho_c + \rho_x}, \quad (4)$$

where H and γ are respectively the Hubble factor and interaction parameter.

The background solution for the densities of dark matter and dark energy are derived from the resolutions of equations (2) and (3) and are expressed as follows:

$$\begin{aligned} \rho_c = & \frac{3H_0^2}{8\pi G} a^{-\frac{3(\omega_x + \omega_x^2 + \gamma)}{\omega_x + \gamma}} \\ & \times \left[\frac{\Omega_{x0}(\omega_x + \gamma) + (\Omega_{c0}\omega_x - \Omega_{x0}\gamma) a^{3\omega_x}}{(\Omega_{c0} + \Omega_{x0})\omega_x} \right]^{-\frac{\gamma}{\omega_x + \gamma}} \\ & \times \left[\Omega_{c0} a^{3\omega_x} + \Omega_{x0} \frac{\gamma}{\omega_x} (1 - a^{3\omega_x}) \right] \end{aligned} \quad (5)$$

¹ The documentation for the code is available at https://github.com/brinckmann/montepython_public/.

² The documentation for the code is available at https://lesgourg.github.io/class_public/class.html.

$$\begin{aligned} \rho_x = & \frac{3H_0^2}{8\pi G} \Omega_{x0} a^{-\frac{3(\omega_x + \omega_x^2 + \gamma)}{\omega_x + \gamma}} \\ & \times \left[\frac{\Omega_{x0}(\omega_x + \gamma) + (\Omega_{c0}\omega_x - \Omega_{x0}\gamma) a^{3\omega_x}}{(\Omega_{c0} + \Omega_{x0})\omega_x} \right]^{-\frac{\gamma}{\omega_x + \gamma}} \end{aligned} \quad (6)$$

where Ω_{x0} and Ω_{c0} are the current DE and DM density parameters. It is possible to express it in a unified way,

$$r(a) = r_0 a^{3\omega_x} + \frac{\gamma}{\omega_x} (1 - a^{3\omega_x}), \quad (7)$$

where $r(a)$ is defined as the ratio between the dark matter density and the dark energy density, $r(a) \equiv \rho_c / \rho_x$. In this case, when $\omega_x < 0$, and in the limit where the scale factor $a(t)$ tends to infinity, $r(a)$ approaches a constant value, which differs from the standard Λ CDM model that tends to zero. Figure 1 shows curves of $r(a)$ for different values of the interaction parameter γ , while Figure 2 shows the density parameter of the energy components, both with the EoS parameter fixed respectively at $\omega_x = -0.8$, $\omega_x = -1$, and $\omega_x = -1.2$.

We are interested in determining the regions where the densities ρ_x and ρ_c are greater than or equal to zero. Specifically, we want to find the allowed regions for the DE and DM densities during their cosmic evolution, as only these have physical significance. Given the definition $r(a) = \rho_c / \rho_x$, it is sufficient to evaluate only one of the pairs: ρ_x, ρ_c or $\rho_x, r(a)$ or $\rho_c, r(a)$. To ensure that the curves have values greater than or equal to zero, from the initial scale factor $a = 0$ to $a \rightarrow \infty$, it is suitable to introduce a variable transformation of the type:

$$y = \frac{2}{\pi} \arctan(\bar{y}), \quad (8)$$

where \bar{y} can be: ρ_c , ρ_x , r , or a . The x-axis, used for the scale factor, assumes the finite interval $x = [0, 1]$, while y , being used for ρ_x , or r , assumes the finite interval $y = [-1, 1]$.

To ensure that equation (6) satisfies $\rho_x \geq 0$, in Figure 3, was plotted $(2/\pi) \arctan(\rho_x)$ versus $(2/\pi) \arctan(a)$ from a computation with 30000 of generated curves with the parameters ω_x , γ , Ω_{m0} , and h (where h is $H/100$ km/s/Mpc) randomly varying between the intervals of $\omega_x = [-2, 2]$, $\gamma = [-2, 2]$, $\Omega_{m0} = [-1, 1]$, and $h = [0.5, 1]$, respectively. Meanwhile, Figure 4 shows the plot of $(2/\pi) \arctan(r)$ versus $(2/\pi) \arctan(a)$, built with the generation of 5000 curves, with the same random choice of the parameters ω_x , γ , Ω_{m0} . In this figure, the dark matter density can assume negative values ($\rho_c < 0$) for certain time intervals (in the past or in the future), thereby violating the WEC. From equation (5), it is possible to assess the conditions leading to the WEC violation. Thus, we can divide the analysis into two distinct periods: the past and the future, so that it can be observed that the energy density of matter assumes negative values at

$$a = \left[\frac{-\gamma \Omega_{x0}}{\omega_x \Omega_{c0} - \gamma \Omega_{x0}} \right]^{\frac{1}{3\omega_x}}. \quad (9)$$

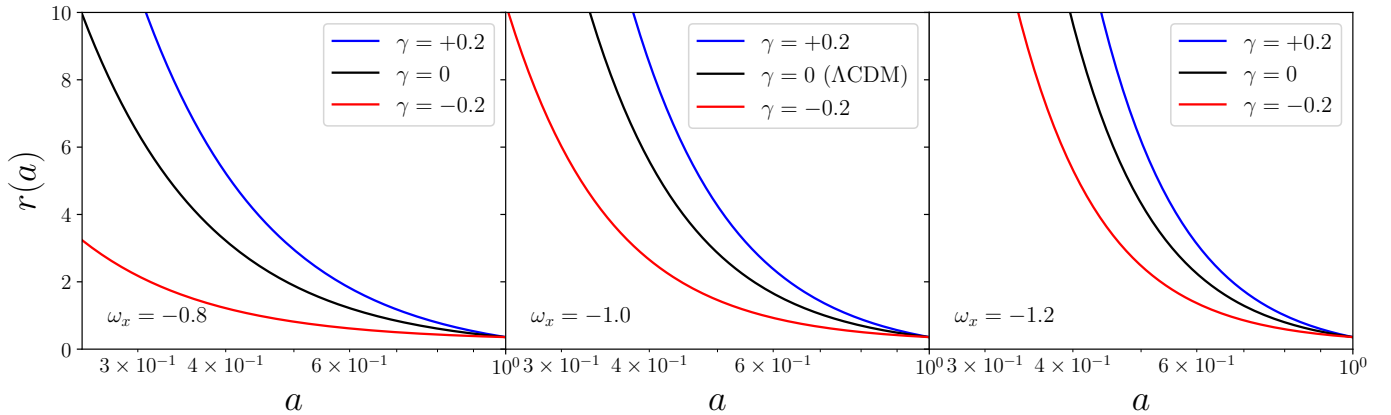


Fig. 1. Ratio between the dark matter density and the dark energy density. Left panel: The black line represents the model with $\gamma = 0$, the red line has $\gamma = -0.2$, and the blue line has $\gamma = +0.2$, with the EoS parameter fixed at $\omega_x = -0.8$. Central panel: The black line represents the model with $\gamma = 0$ (non-interacting case, i.e., reduces to the Λ CDM model), the red line has $\gamma = -0.2$, and the blue line has $\gamma = +0.2$, with the EoS parameter fixed at $\omega_x = -1$. Right panel: The black line represents the model with $\gamma = 0$, the red line has $\gamma = -0.2$, and the blue lines have $\gamma = +0.2$, with the EoS parameter fixed at $\omega_x = -1.2$. In all panels, DE density parameter was fixed at $\Omega_{x0} = 0.7$.

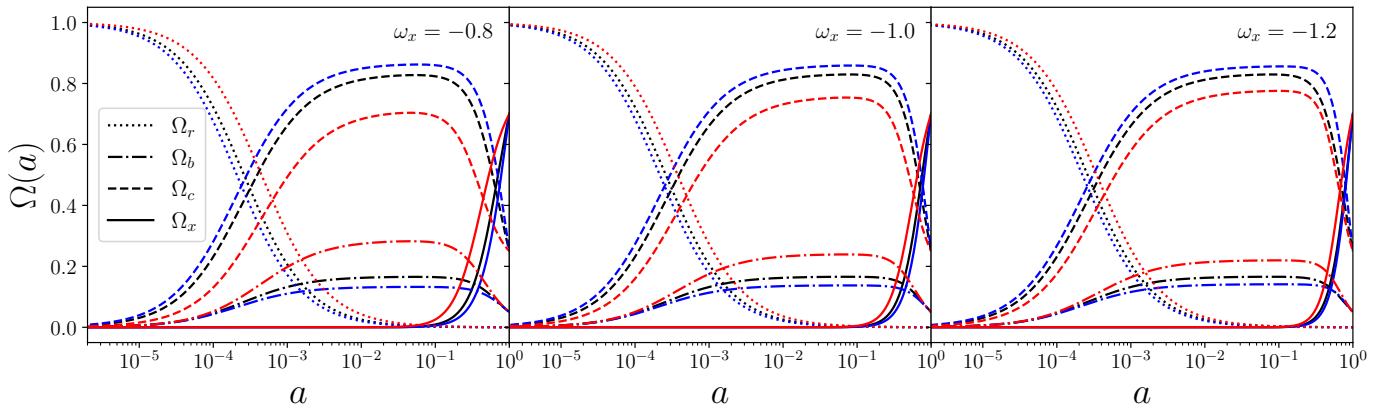


Fig. 2. Evolution of the density parameters of the Universe's components as a function of the scale factor. The EoS parameter was fixed respectively at $\omega_x = -0.8$ (left panel), $\omega_x = -1$ (central panel), and $\omega_x = -1.2$ (right panel). In all panels, the dotted line represents the radiation component, the dashed line represents dark matter, the dash-dotted line represents baryons, and the solid line represents the dark energy component. The black lines represent the model with $\gamma = 0$, the red lines have $\gamma = -0.2$, and the blue lines have $\gamma = +0.2$.

Assuming that the value of the equation of state parameter is $\omega_x < 0$, we straightly obtain the solution conditions for the equation (9) in the intervals $0 < a < 1$ (in the past) and $a > 1$ (in the future). To prevent the dark matter energy density from becoming negative in the early moments of the universe, the interaction parameter must satisfy the following condition

$$\gamma > -|\omega_x| \frac{\Omega_{c0}}{\Omega_{x0}}. \quad (10)$$

However, it is likely that the density of dark matter, ρ_c , will be negative in the future, unless,

$$\gamma \leq 0, \quad (11)$$

that is independent of the value ω_x . The equations (10) and (11) define the range in which the model is physically well-defined, regardless of the timescale. In Figure 5, the

scale factor is depicted for the WEC violation as a function of the interaction parameter γ .

Let's consider, for example, $\omega_x = -1$, $\Omega_{x0} = 0.7$ and $\gamma = 0.2$ ρ_c becomes negative with scale factor $a \approx 1.4$, where the critical density is $\rho_{cr0} = \frac{3H_0^2}{8\pi G} = 1.87798 \times 10^{-26} h^2 \frac{\text{kg}}{\text{m}^3}$, with $h = 0.7324$ [24]. Figure 6 shows how the universe evolves with the Hubble function, DE, and matter densities as a function of the scale factor.

3 Perturbations

The description of the dark sector interaction for an interacting model, assuming a phenomenological nature, can be given through a covariant derivative of the energy-momentum tensor, where the equations for conserved baryons,

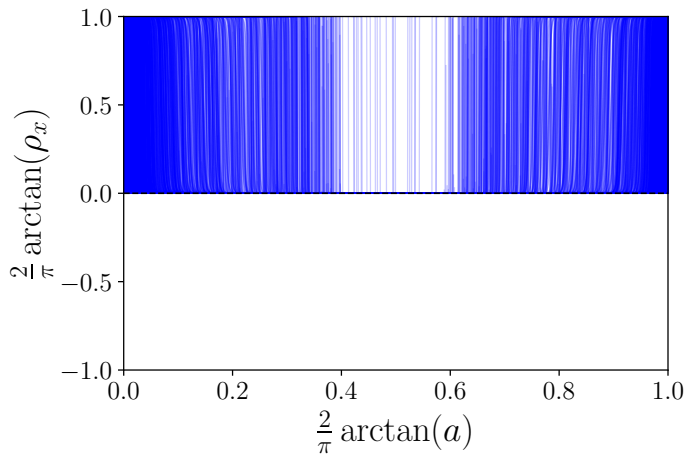


Fig. 3. Computation with 30000 of curves of $\rho_x(a)$. The blue lines represent curves with values $\rho_x(a) \geq 0$. There were no curves for $\rho_x(a) < 0$. The graph represents the largest possible scale for ρ_x and a ($\rho_x = [-\infty, \infty]$, $a = [0, \infty]$), with the parameters ω_x , γ , Ω_{m0} , and h randomly varying between the intervals of $\omega_x = [-2, 2]$, $\gamma = [-2, 2]$, $\Omega_{m0} = [-1, 1]$, and $h = [0.5, 1]$, respectively.

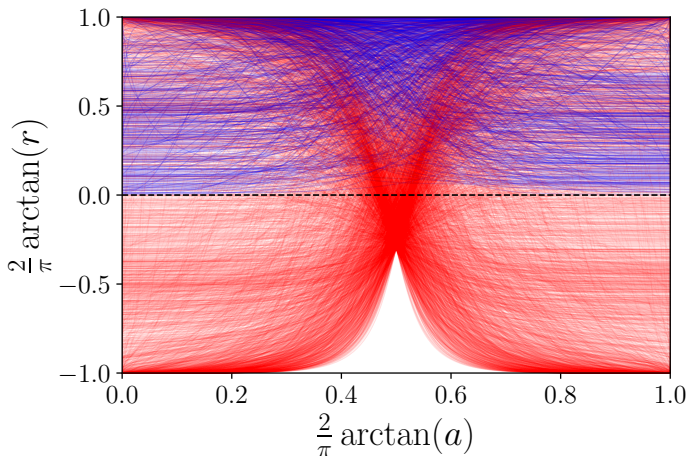


Fig. 4. Computation with 5000 of curves of $r(a)$. The blue lines represent curves with values $r(a) \geq 0$, and the red lines represent curves with values that, at some point, have $r < 0$. The graph represents the largest possible scale for r and a ($r = [-\infty, \infty]$, $a = [0, \infty]$), with the parameters ω_x , γ , and Ω_{m0} randomly varying between the intervals of $\omega_x = [-2, 2]$, $\gamma = [-2, 2]$, and $\Omega_{m0} = [-1, 1]$, respectively.

DM and DE are

$$T_{b;\nu}^{\mu\nu} = 0, \quad (12)$$

$$T_{c;\nu}^{\mu\nu} = Q^\mu, \quad (13)$$

and

$$T_{x;\nu}^{\mu\nu} = -Q^\mu. \quad (14)$$

The term Q^μ is a four-vector that acts as a source for the energy-momentum tensor; the terms $T_c^{\mu\nu}$ and $T_x^{\mu\nu}$ are

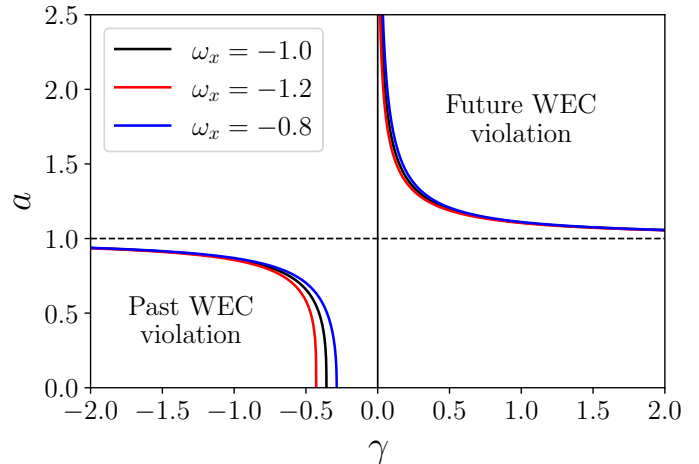


Fig. 5. Plot of the scale factor a that violates the WEC as a function of the interaction parameter γ . On the top right is shown the WEC violation in the future, while on the bottom left is shown the WEC violation in the past. The black line corresponds to $\omega_x = -1$, while the blue line corresponds to $\omega_x = -0.8$, and the red line corresponds to $\omega_x = -1.2$. Here, the dark energy density parameter was fixed at $\Omega_{x0} = 0.7$.

the energy-momentum tensors for dark matter and dark energy, respectively. In a perfect fluid, the spatial components for a covariant derivative of the energy-momentum tensor are zero. Consequently, in the background, the interaction term is given by a scalar function is $Q^\mu = (Q, \vec{0})$ in an unperturbed case (as seen in the previous section) [10, 17, 25, 26]. On the other hand, for a perturbed case and assuming scalar perturbations responsible for the formation of structures in the universe, the perturbed Friedmann-Lemaître-Robertson-Walker metric in a spatially flat universe considering the Newtonian gauge is given by [10, 27]

$$ds^2 = a^2(\tau) [-(1 + 2\psi) d\tau^2 + (1 - 2\phi) dx^i dx_i] \quad (15)$$

with the scalar degrees of freedom being ψ and ϕ , and using conformal time τ instead of cosmic time t .

In describing structure formation at the linear level, it is necessary to solve all the perturbation equations for each component of the universe. The temperature anisotropies of the CMB are derived by solving the Boltzmann equations for all components [27]. However, assuming that the baryon and radiation components are similar to those in the Λ CDM model, they interact with each other via Thomson scattering before recombination and are not directly connected to the dark sector [10, 27, 28].

Assuming a fluid dynamic description to represent the dark sector components, the perturbed fluid equations must incorporate the contribution of the interaction term. Thus, we can consider at the linear level the perturbative contribution divided into two components, one parallel and one orthogonal to the four-velocity,

$$Q^\mu = Qu^\mu + F^\mu, \quad (16)$$

with $F^\mu u_\mu = 0$. The first term on the right-hand side Q is a scalar function with background components de-

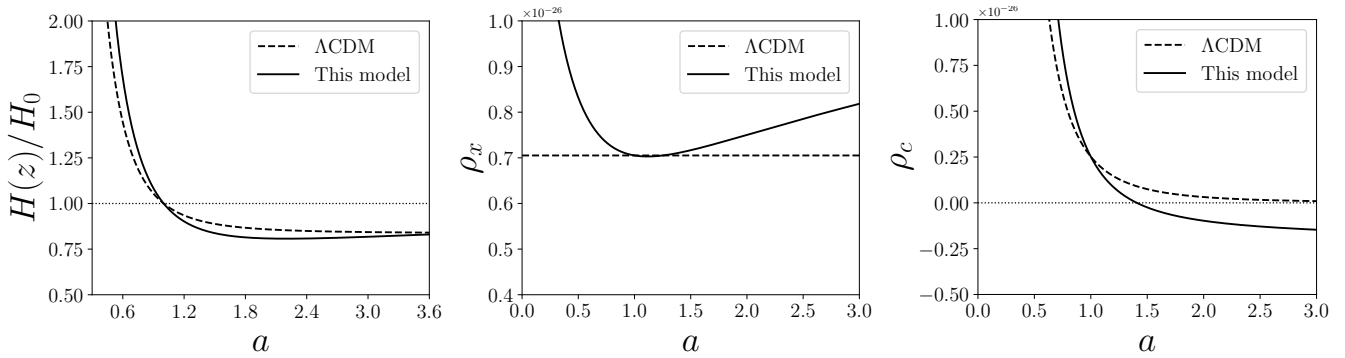


Fig. 6. Background solutions of this model and the Λ CDM model as a function of the scale factor a . Left panel: Shows the Hubble function $H(z)/H_0$. Central panel: Dark energy density. Right panel: Dark matter density. In all panels, the solid line corresponds to the model, with $\omega_x = -1$, $\Omega_{x0} = 0.7$, $\gamma = 0.2$ and $h = 0.7324$, and the dashed lines correspond to the Λ CDM model, with the same values of Ω_{x0} and h .

defined in equations (2) and (3). The perturbative contribution will be denoted by \hat{Q} and has the form $\hat{Q} = \hat{\Theta}\gamma R + 3H\gamma\hat{R}$, where \hat{R} is model dependent and can be obtained by linearizing the expansion scalar $\Theta \equiv u^\mu{}_{;\mu}$, in Newtonian gauge it is expressed by

$$\hat{\Theta} = \frac{1}{a} (\theta_{tot} - \Theta\psi - 3\phi'), \quad (17)$$

where θ_{tot} is the divergence of the interacting fluid for the entire cosmic medium. The ideal fluid description of the dark sector components requires that the term F^μ has only a spatial perturbative contribution. Therefore, the total perturbative interaction term can be written as $\hat{Q}^\mu = a (Q\psi + \hat{Q}, Q\hat{u}^i + F^i)$.

In considering the basic equations of the energy balance defined in Eqs. (13) and (14), taking into account a general interacting fluid with constant EoS $p = \omega\rho$ and perturbed four-velocity $\hat{u}^\mu = a^{-1} (-\psi, \partial^i v)$, where v is its peculiar velocity. The conservation of energy and momentum in the Newtonian gauge is given by

$$\begin{aligned} & \delta' + 3\mathcal{H} (c_s^2 - \omega) \delta + 9\mathcal{H}^2 (1 + \omega) (c_s^2 - c_a^2) \frac{\theta}{k^2} \\ & + (1 + \omega) (\theta - 3\phi') \\ & = \frac{Qa}{\rho} \left[\frac{\hat{Q}}{Q} - \delta + \psi + 3\mathcal{H} (c_s^2 - c_a^2) \frac{\theta}{k^2} \right], \end{aligned} \quad (18)$$

$$\begin{aligned} & \theta' + \mathcal{H} (1 - 3c_s^2) \theta - \frac{k^2 c_s^2}{1 + \omega} \delta - k^2 \psi \\ & = \frac{a}{\rho(1 + \omega)} [Q\theta_{tot} - k^2 f - (1 + c_s^2) Q\theta]. \end{aligned} \quad (19)$$

In the above equations, primes denote derivatives with respect to conformal time, where \mathcal{H} is the Hubble parameter in conformal time, defined as $\mathcal{H} = aH$. In equation (18) the density contrast $\delta \equiv \hat{\rho}/\rho$ is introduced, where $\hat{\rho}$ is the perturbative energy density and ρ is the background energy density. In equation (19), the dynamical quantity of interest is the divergence of the interacting

fluid $\theta \equiv i k^a \partial_a v$. Meanwhile, θ_{tot} denotes the same quantity, but for the entire cosmic medium, not limited to a single fluid. For scalar perturbations, it is useful to define the spatial contribution of the interaction term as $aF^i = \partial^i f$. Finally, c_a^2 and c_s^2 correspond to the adiabatic sound speed and the physical rest-frame sound speed for the fluid, respectively. Under the assumption of a constant EoS parameter, the adiabatic sound speed c_a^2 reduces to ω .

Now, using the equations (18) and (19), we can write the perturbative equations for the dark sector components. For the CDM component, we have

$$\delta'_c + \theta_c - 3\phi' = \frac{aQ}{\rho_c} \left(\delta_c - \frac{\hat{Q}}{Q} - \psi \right), \quad (20)$$

$$\theta'_c + \mathcal{H}\theta_c - k^2\psi = \frac{aQ}{\rho_c} (\theta_{tot} - \theta_c). \quad (21)$$

While for the DE component, it is expressed as

$$\begin{aligned} & \delta'_x + (1 + \omega_x) (\theta_x - 3\phi') + 3\mathcal{H} (c_s^2 - \omega_x) \delta_x \\ & = -\frac{aQ}{\rho_x} \left(\delta_x - \frac{\hat{Q}}{Q} \right), \end{aligned} \quad (22)$$

$$\begin{aligned} & \theta'_x + \mathcal{H} (1 - 3c_s^2) \theta_x - \frac{c_s^2 k^2}{1 + \omega_x} \delta_x - k^2 \psi \\ & = \frac{aQ}{(1 + \omega_x)\rho_x} \left[\theta_{tot} - (1 + c_s^2)\theta_x + (1 + \omega_x) \frac{\hat{Q}}{Q} \right]. \end{aligned} \quad (23)$$

To prevent instabilities, the physical speed of sound c_s^2 must not be negative in dynamical dark energy. Thus, we consider $c_s^2 = 1$, in agreement with several references [10, 28, 29, 30].

The perturbative interaction term is given by the linearization of the background interaction term (Eq. 4), which is expressed as [10]

$$\hat{Q} = Q \left(\frac{\hat{\Theta}}{\Theta} + \frac{\rho_x \delta_x + 2\rho_c \delta_x - \rho_c \delta_c}{\rho_c + \rho_x} \right). \quad (24)$$

In the background, the expansion scalar Θ simplifies to $\Theta = 3H$ [10,31].

4 Methodology

This section briefly describes the observational datasets and the statistical analysis methodology.

4.1 Observational Data

Here we will present the observational datasets.

- **Type Ia Supernovae (SNe Ia):** SNe Ia are considered standard candles in astronomy and have played a pivotal role in observing the Universe’s accelerated expansion [32,1,2,3]. In general, the apparent magnitude and luminosity distance are related by $m = 5 \log(D_L) + 25 + M$, where M is the absolute magnitude. $D_L(z)$ represents the luminosity distance expressed in units of Mpc. In this analysis, 1048 measurements of apparent magnitudes from Type Ia supernovae were used, referred to as the Pantheon sample³. This dataset covers the redshift range $0.01 < z < 2.3$ [33,34].
- **Current Value of the Hubble Expansion Rate (H_0):** The Hubble expansion rate obtained by [24] provides the best estimate of $H_0 = (73.24 \pm 1.74)$ km s⁻¹ Mpc⁻¹, from a set of observations containing more than 600 Cepheids, using both infrared and visible frequencies. This value is independent of the cosmological model.
- **Cosmic Chronometers (CC):** The Cosmic Chronometers are independent data from cosmological models, derived from measurements taken from ancient galaxies. There are 30 measurements of $H(z)$ in the range $0.07 < z < 1.965$, as presented in Table 1 [35].⁴
- **Baryon Acoustic Oscillations (BAO):** Baryon Acoustic Oscillations carry information from the pre-decoupling Universe. The baryon-photon fluid propagates with an acoustic velocity described as follows [41,42]:

$$c_s = \frac{c}{\sqrt{3(1+R)}}, \quad (25)$$

with $R \equiv \frac{3\rho_b}{4\rho_\gamma} \propto \frac{\Omega_b}{1+z}$.

After decoupling, photons begin to travel with a characteristic scale given by

$$r_s(a_{\text{drag}}) \equiv \int_0^{a_{\text{drag}}} \frac{c_s(a)}{Ha^2} da, \quad (26)$$

where c_s represents the speed of sound in the primordial plasma and a_{drag} is the scale factor at the

³ The Pantheon data is available and can be downloaded from <http://www.github.com/dscolnic/Pantheon>.

⁴ The CC data has been included in MontePython and is available at https://github.com/brinckmann/montepython_public/tree/3.3/data/cosmic_clocks.

Table 1. Measurements of $H(z)$, with their respective errors, containing the CC data.

z	$H(z)$	$\sigma_{H(z)}$	References
0.07	69.0	19.6	[36]
0.09	69.0	12.0	[37]
0.12	68.6	26.2	[36]
0.17	83.0	8.0	[37]
0.179	75.0	4.0	[38]
0.199	75.0	5.0	[38]
0.2	72.9	29.6	[36]
0.27	77.0	14.0	[37]
0.28	88.8	36.6	[36]
0.352	83.0	14.0	[38]
0.3802	83.0	13.5	[35]
0.4	95.0	17.0	[37]
0.4004	77.0	10.2	[35]
0.4247	87.1	11.2	[35]
0.4497	92.8	12.9	[35]
0.4783	80.9	9.0	[35]
0.48	97.0	62.0	[39]
0.593	104.0	13.0	[38]
0.68	92.0	8.0	[38]
0.781	105.0	12.0	[38]
0.875	125.0	17.0	[38]
0.88	90.0	40.0	[39]
0.9	117.0	23.0	[37]
1.037	154.0	20.0	[38]
1.3	168.0	17.0	[37]
1.363	160.0	33.6	[40]
1.43	177.0	18.0	[37]
1.53	140.0	14.0	[37]
1.75	202.0	40.0	[37]
1.965	186.0	50.4	[40]

drag time, referring to the moment in the early universe when photons and baryons (protons and neutrons) decoupled [43]. The isotropic BAO measurements are provided through the dimensionless ratio $D_V/r_s(a_{\text{drag}})$, where D_V is the geometric mean that combines the scales of the line-of-sight and transverse distances. D_V is expressed by [44,45]

$$D_V(z) = \left[(1+z)^2 D_A^2(z) \frac{cz}{H(z)} \right]^{1/3}, \quad (27)$$

where $D_A(z)$ is the angular diameter distance. Here, the BAO data⁵ is obtained from Refs. [46,47,48].

- **CMB data (Planck):** The data used here for CMB are measurements from Planck 2018, which include information on temperature, polarization, temperature polarization cross-correlation spectra, and lensing maps reconstruction, Planck (TT, TE, EE+lowE+lensing) [49].⁶ In these analyses, the standard likelihood codes

⁵ The BAO data can be found from the likelihoods added to MontePython, which reference the respective data files that are available at https://github.com/brinckmann/montepython_public/tree/3.6/montepython/likelihoods.

⁶ For CMB analysis, all Planck likelihood codes and data can be obtained at <https://pla.esac.esa.int/pla/>.

were considered: (i) COMANDER for the low- l TT spectrum, with spectrum data ranging from $2 \leq l < 30$; (ii) SimAll for the low- l EE spectrum, with spectrum data ranging from $2 \leq l < 30$; (iii) Plik TT, TE, EE for the TT, TE, and EE spectra, covering $30 \leq l \lesssim 2500$ for TT and $30 \leq l \lesssim 2000$ for TE and EE; (iv) lensing power spectrum reconstruction with $8 \leq l \leq 400$. For more details on the likelihoods, see Refs. [49,32].

4.2 Statistical analysis

Statistical analysis is performed using the MontePython code [50,51], which utilizes the CLASS code [52,51]. In the MontePython code, the Markov Chain Monte Carlo (MCMC) method [53,54] is used to perform statistical analysis on the input data, comparing it with the theoretical predictions, that are provided by a suitably modified version of the CLASS code, to take into account the cosmology framework described in section 2. To use the Λ CDM and ω CDM models, no modifications are necessary in the code. However, for other models, such as the interacting models, it is necessary to implement the background equations as well as the perturbed fluid equations with the linear perturbative contribution of the model in the code. For all chains, during the MCMC analysis in MontePython, it is required that the Gelman-Rubin convergence parameter satisfies the condition $\hat{R}-1 < 0.01$ [55, 56]. We utilized `GetDist`⁷ to analyze and plot the chains [57,58]. It allows for creating contour plots, histograms, parameter correlations, among others, from datasets generated by codes such as MontePython. In this part, using the `GetDist` library, the samples where the parameter γ does not satisfy the conditions of equations (10) and (11) were filtered. These equations establish specific limits for the value of γ . Thus, only the samples that adhere to these restrictions are considered in the posterior analysis, specifically with the prior applied.

4.3 Combination of dataset

We investigate the impact of the physical or WEC prior, in the case of $\gamma \geq 0$, on the estimation of the cosmological parameters of the model under analysis. The unmodified CLASS code already automatically resolves past WEC violation. A Bayesian statistical analysis was conducted with and without the inclusion of such a prior, for five different datasets:

1. Background: *Composed of SNe Ia, CC, and BAO data;*
2. Background+ H_0 : *Composed of SNe Ia, CC, BAO, and H_0 data;*
3. Planck: *Composed of the full CMB data from Planck, combined with Planck TTTEEE+lensing reconstruction;*

4. Background+Planck: *Composed of the combination of Planck+Background;*
5. Background+Planck+ H_0 : *Composed of the combination of Planck+Background, with H_0 .*

5 Results and discussion

When we do not include the Planck data in our analysis, we considered the following cosmological parameters: $\mathcal{P}=\{\omega_c, H_0, \gamma\}$ where ω_c is the cold dark matter density parameter, and the derived parameters: $\mathcal{P}'=\{\Omega_{m0}, \omega_b\}$ where ω_b and Ω_{m0} represent respectively the baryon and current matter density parameters. Otherwise when we include the data from Planck, the parameters are: $\mathcal{P}=\{100\theta_s, n_s, \ln(10^{10}A_s), \omega_b, \omega_c, \tau_{reio}, \gamma\}$ where $100\theta_s$, n_s , $\ln(10^{10}A_s)$, and τ_{reio} are respectively the angular size of the sound horizon (scaled by 100), the scalar spectral index, the logarithm of the amplitude of the primordial scalar power spectrum, and the optical depth to reionization, and the derived parameters: $\mathcal{P}'=\{H_0, \Omega_{m0}, \sigma_8, S_8\}$, where σ_8 and S_8 are respectively the standard deviation of the density fluctuation in an $8 h^{-1}$ Mpc radius sphere, and the structure growth parameters, with the equation of state parameter fixed at $\omega_x = -1$. The results of our analysis are presented in Tables 2 and 3, both with and without the WEC prior. For the background tests, the baryon density parameter was fixed at 0.05, while in the analyses that include CMB data, Ω_{b0} is a free parameter.

In Figure 7, the contour curves without the implementation of the WEC constraint in the background solutions are shown. In Figure 8, the contour curves taking into account the WEC constraint are presented. Both figures display contour regions at 1σ and 2σ confidence level (C.L.), respectively. Figure 9 shows posteriors for several parameters without the use of a WEC prior. Figure 10 shows posteriors for several parameters with the use of a WEC prior. The confidence regions for H_0 , Ω_{m0} and σ_8 are less restrictive without the WEC prior and more restrictive with it, being consistent with the Planck results [32] at 2σ C.L.. Figures 7 and 8 show an anticorrelation between the interaction parameter γ and the parameter Ω_{m0} , and exhibits a correlation between the interaction parameter γ and the parameters σ_8 , S_8 and H_0 . To interpret these correlations, it is useful to observe how the observables change as the involved parameters vary.

In Figure 11 are shown the expansion rate $H(z)$ (top panel) and the luminosity distance $D_L(z)$ (bottom panel) as a function of redshift for different values of γ . Even if we only consider the background, we can appreciate a compensatory effect between γ and Ω_{m0} . As Ω_{m0} increases, the growth of the Hubble parameter, which is related to the data of cosmic chronometers, decreases, since, in the absence of curvature, the contribution of dark energy increases. Since the smaller the γ parameter, the greater the suppression of the dark matter energy density contribution (see Fig. 2), we find an anticorrelation between Ω_m and the interaction parameter. Consequently, the cor-

⁷ The documentation for the code is available at <https://getdist.readthedocs.io/>.

Table 2. Statistical analysis results at 1σ C.L., considering the analyses without and with the WEC prior, using the datasets: Background and Background+ H_0 .

Parameter	Background		Background+ H_0	
	No prior	WEC prior	No prior	WEC prior
γ	$-0.02^{+0.11}_{-0.11}$	$-0.088^{+0.071}_{-0.041}$	$-0.02^{+0.11}_{-0.11}$	$-0.095^{+0.084}_{-0.040}$
ω_c	$0.124^{+0.017}_{-0.015}$	$0.132^{+0.010}_{-0.012}$	$0.124^{+0.017}_{-0.015}$	$0.134^{+0.010}_{-0.012}$
H_0	$69.1^{+1.7}_{-1.7}$	$68.6^{+1.3}_{-1.3}$	$69.1^{+1.7}_{-1.7}$	$68.3^{+1.4}_{-1.4}$
ω_b	$0.0239^{+0.0012}_{-0.0012}$	$0.02352^{+0.00082}_{-0.00094}$	$0.0239^{+0.0012}_{-0.0012}$	$0.0236^{+0.00095}_{-0.00095}$
Ω_{m0}	$0.310^{+0.040}_{-0.040}$	$0.334^{+0.018}_{-0.028}$	$0.310^{+0.041}_{-0.041}$	$0.338^{+0.022}_{-0.028}$

Table 3. Statistical analysis results at 1σ C.L., considering the analyses without and with the WEC prior, using the datasets: Planck, Planck+Background, and Planck+Background+ H_0 .

Parameter	Planck		Planck+Background		Planck+Background+ H_0	
	No prior	WEC prior	No prior	WEC prior	No prior	WEC prior
γ	$0.08^{+0.14}_{-0.11}$	$-0.078^{+0.070}_{-0.039}$	$0.062^{+0.070}_{-0.070}$	$-0.036^{+0.034}_{-0.020}$	$0.123^{+0.071}_{-0.071}$	$-0.031^{+0.029}_{-0.019}$
$100\theta_s$	$1.04191^{+0.00030}_{-0.00030}$	$1.04187^{+0.00030}_{-0.00030}$	$1.04197^{+0.00028}_{-0.00028}$	$1.04206^{+0.00028}_{-0.00024}$	$1.04200^{+0.00028}_{-0.00028}$	$1.04208^{+0.00027}_{-0.00027}$
$\ln 10^{10}A_s$	$3.045^{+0.015}_{-0.015}$	$3.044^{+0.014}_{-0.014}$	$3.046^{+0.012}_{-0.014}$	$3.048^{+0.011}_{-0.016}$	$3.047^{+0.011}_{-0.014}$	$3.049^{+0.012}_{-0.015}$
n_s	$0.9654^{+0.0041}_{-0.0041}$	$0.9647^{+0.0040}_{-0.0040}$	$0.9669^{+0.0037}_{-0.0037}$	$0.9680^{+0.0037}_{-0.0037}$	$0.9674^{+0.0037}_{-0.0037}$	$0.9693^{+0.0032}_{-0.0032}$
ω_b	$0.02238^{+0.00014}_{-0.00014}$	$0.02236^{+0.00014}_{-0.00014}$	$0.02240^{+0.00014}_{-0.00014}$	$0.02244^{+0.00014}_{-0.00014}$	$0.02245^{+0.00014}_{-0.00014}$	$0.02251^{+0.00015}_{-0.00015}$
ω_c	$0.104^{+0.022}_{-0.022}$	$0.1287^{+0.0054}_{-0.0054}$	$0.108^{+0.014}_{-0.011}$	$0.1238^{+0.0033}_{-0.0041}$	$0.096^{+0.014}_{-0.014}$	$0.1216^{+0.0016}_{-0.0030}$
τ_{reio}	$0.0544^{+0.0076}_{-0.0076}$	$0.0539^{+0.0070}_{-0.0070}$	$0.0557^{+0.0061}_{-0.0072}$	$0.0571^{+0.0070}_{-0.0070}$	$0.0562^{+0.0073}_{-0.0073}$	$0.0583^{+0.0067}_{-0.0067}$
H_0	$68.2^{+1.5}_{-1.3}$	$66.70^{+0.70}_{-0.70}$	$68.24^{+0.62}_{-0.71}$	$67.57^{+0.43}_{-0.43}$	$68.99^{+0.65}_{-0.65}$	$67.85^{+0.42}_{-0.42}$
Ω_{m0}	$0.275^{+0.058}_{-0.066}$	$0.347^{+0.020}_{-0.027}$	$0.282^{+0.034}_{-0.029}$	$0.323^{+0.013}_{-0.015}$	$0.251^{+0.033}_{-0.033}$	$0.318^{+0.010}_{-0.010}$
σ_8	$0.93^{+0.14}_{-0.17}$	$0.763^{+0.036}_{-0.029}$	$0.879^{+0.055}_{-0.095}$	$0.783^{+0.023}_{-0.015}$	$0.964^{+0.091}_{-0.130}$	$0.785^{+0.021}_{-0.015}$
S_8	$0.869^{+0.041}_{-0.057}$	$0.819^{+0.015}_{-0.015}$	$0.848^{+0.022}_{-0.036}$	$0.813^{+0.010}_{-0.012}$	$0.872^{+0.034}_{-0.047}$	$0.809^{+0.010}_{-0.012}$

relation between γ and the Hubble constant is straightforward, as $H(z)$ increases with H_0 . Similarly, the luminosity distance related to type Ia supernova data, since it incorporates the integral of $H(z)^{-1}$, increases with increasing Ω_{m0} parameter (or decreases with increasing H_0), just as it decreases with increasing the γ parameter. It is possible to repeat the same evaluation for the angular distance D_A , related to the BAO data, since $D_L = (1+z)^2 D_A$.

Figure 12 shows the temperature power spectrum as the parameter γ varies, where it is possible to compare this behavior with that observed with changes in the parameter Ω_{m0} e σ_8 . An increase in the value of Ω_{m0} brings forward the radiation epoch (see Figure 2), and through radiation driving, suppresses the power spectrum [59, 60]. Similarly, an increase in the parameter γ also brings forward the radiation epoch, producing the same effect. Conversely, an increase in the σ_8 parameter corresponds to an increase in the amplitude of the scalar perturbations, or to an increase in the temperature anisotropies. This implies that in order to fit the data relating to the temperature fluctuations of the cosmic microwave background, we find an anticorrelation between the parameter γ and the parameter Ω_{m0} and a correlation with the parameter σ_8 and therefore with the parameter S_8 .

Note that the same trends accompany other models that exhibit similar coupling physics [61, 10].

In Figure 13, the posterior results for the interaction parameter γ are presented in two scenarios: without the use of a prior (left panel) and with the application of the WEC prior (right panel). For the case without prior, only when Planck data is not used, the mean value of γ is negative, which prevents the violation of the WEC. On the other hand, when Planck data is used in the analysis, the mean value of γ is slightly greater than zero, which means that the WEC will inevitably be violated in the future. In contrast, when the WEC prior is taken into account, the mean value of γ is always negative, satisfying the WEC.

The results with WEC prior at 1σ C.L. for γ do not satisfy the standard Λ CDM model. In all cases, the Λ CDM limit ($\gamma = 0$) is satisfied within the 2σ C.L..

The right top panels of Figures 9 and 10 show the posteriors for H_0 . Both for the case with the WEC prior and for the one without it, when the datasets Background, Background+ H_0 , and Planck are used there are weaker constraints on the Hubble constant, with a best-fit mean around $H_0 \approx 68.5 - 68.8 \text{ km s}^{-1} \text{ Mpc}^{-1}$, highlighting the need to add more data to these analyses. By combining Background data with Planck data, the constraints are improved. In Appendix A, we reproduced the H_0 tension between the analysis that includes the Planck data and the analysis that includes the background data only in the case of Λ CDM model ($\gamma = 0$) (see Fig. 18). We noted

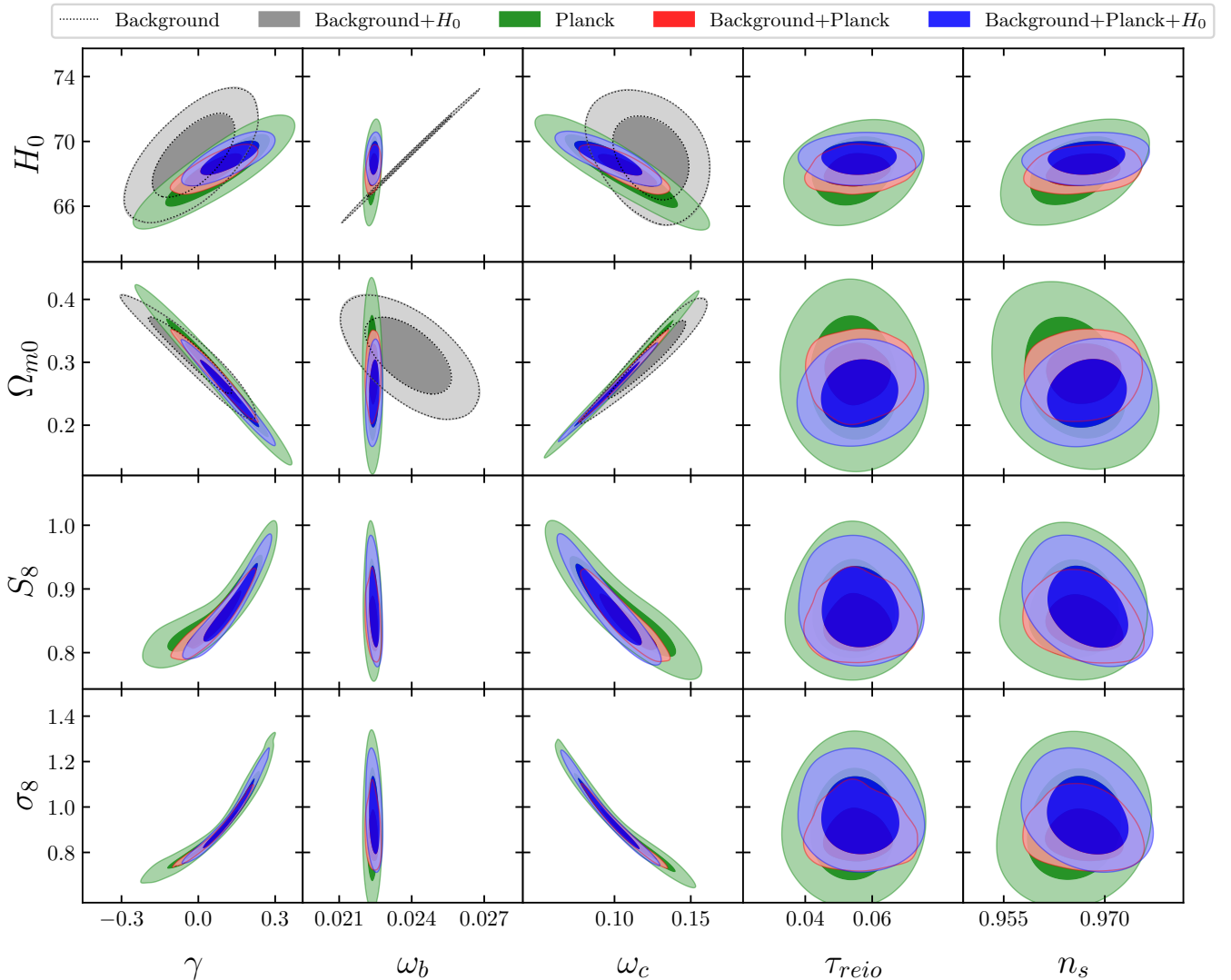


Fig. 7. Rectangular plot with the free cosmological parameters, considering the analyses with WEC prior, using the datasets: Background, Background+ H_0 , Planck, Background+Planck and Background+Planck+ H_0 .

that the tension is attenuated, especially in the case when the WEC prior is ignored.

In Figure 14, the plot for the plane $\sigma_8 - H_0$ is shown. In the case where the WEC prior was not used the constraints are weaker, while in the case the prior was adopted, the constraints are more stringent, and the estimates tend toward to lower value of σ_8 .

The results of the analyses with the WEC prior yield average values of approximately 67.4 and 0.78 for H_0 and σ_8 , respectively. The preference for lower values of σ_8 alleviates the σ_8 tension between the primary CMB results from Planck 2018 [32] and the weak gravitational lensing observations from the KiDS-1000 cosmic shear survey [62].

Figure 15 shows the plot of the interaction parameter γ versus the matter density parameter Ω_{m0} with and without the WEC prior. In the case without the WEC prior, all datasets have weak constraints on the parameters γ and Ω_{m0} , which appear to improve when the Back-

ground and H_0 data are combined with the Planck data. The inclusion of the WEC prior significantly improves the constraints of the parameters, resulting in higher values of Ω_{m0} , which helps to alleviate the S_8 tension between the Planck CMB results and the estimates from the KiDS cosmic shear survey, as discussed in Refs. [32, 62, 63, 64].

Finally, in Figure 16, we present estimates of the quantity $S_8 = \sigma_8 (\Omega_{m0}/0.3)^{1/2}$, with and without the WEC prior, using the datasets that include Planck. The results of the analyses without the WEC prior have weak constraints for S_8 and Ω_{m0} . In contrast, the analyses with the WEC prior present good constraints, with mean values around 0.814 and 0.329 for S_8 and Ω_{m0} , respectively. These results are in agreement at 2σ with the Planck 2018 results [32] for the Λ CDM model, and are also consistent with the results of weak gravitational lensing data from KiDS-1000 [62], as well as clustering and lensing data from the Dark Energy Survey [65, 66] at $\sim 3.5\sigma$ C.L.. The

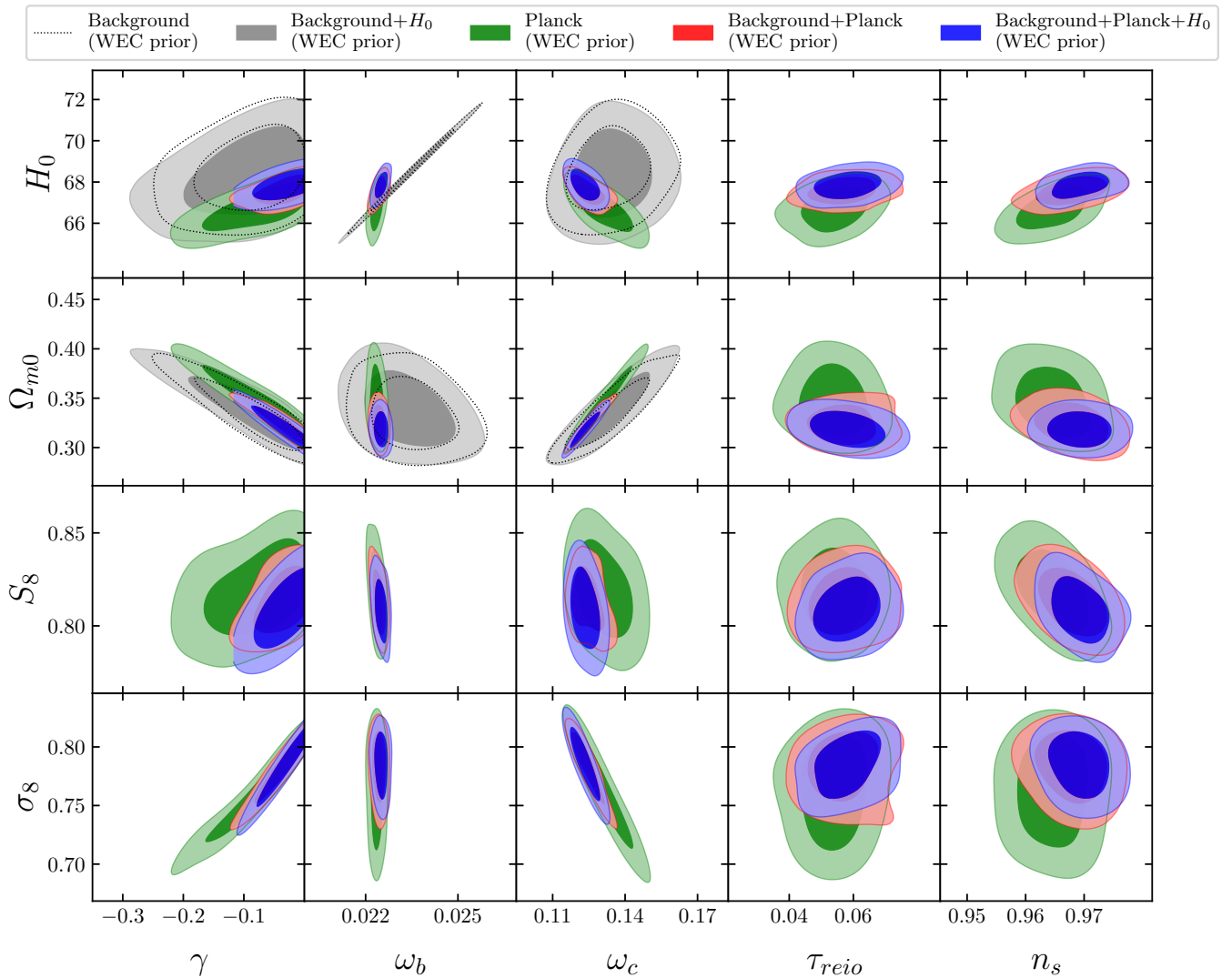


Fig. 8. Rectangular plot with the free cosmological parameters, considering the analyses with WEC prior, using the datasets: Background, Background+ H_0 , Planck, Background+Planck and Background+Planck+ H_0 .

analyses with the WEC prior are also compatible with the results of the analyses for the Λ CDM model (see Appendix A, Tab. 5) at 1.2σ C.L.

6 Conclusions

The standard model Λ CDM presents different problems, such as the cosmological constant problem, the cosmic coincidence, and the Hubble constant tension [5, 6, 7, 8, 9, 10, 11, 13, 14, 15], in this sense, several models and approaches have been proposed to better describe the nature of dark energy. Consequently, several interacting models have been suggested to capture possible interactions between the components of the dark sector of the universe. In this article, we explored an interacting model described by an interacting term proportional to $\rho_x^2 / (\rho_c + \rho_x)$. The direction of the energy transfer depends on the sign of Q : when $Q < 0$, the process of dark matter creation is

enhanced and dark energy decays, whereas when $Q > 0$, the opposite occurs. Here, we investigate the theoretical consistency of this class of cosmologies and show that for positive values of γ ($\gamma > 0$), which physically corresponds to an energy transfer from dark matter to dark energy, this particular model predicts a violation of the WEC, specifically a violation of $\rho_c \geq 0$, which will inevitably occur in the future evolution.

The analysis of the results was executed using the CLASS, MontePython, and GetDist codes, employing five different datasets, as described in Section 4. For all datasets, the results with the WEC prior showed negative values of γ at 1σ C.L., so excluding the standard Λ CDM model, which is reproduced by $\gamma = 0$. However, for the 2σ C.L. regions, the interaction parameter $\gamma = 0$, hence the Λ CDM model is preferred.

Our results showed a notable anticorrelation between the interaction parameter γ and Ω_{m0} , as well as a correlation between γ and the parameters σ_8 , S_8 , and H_0 .

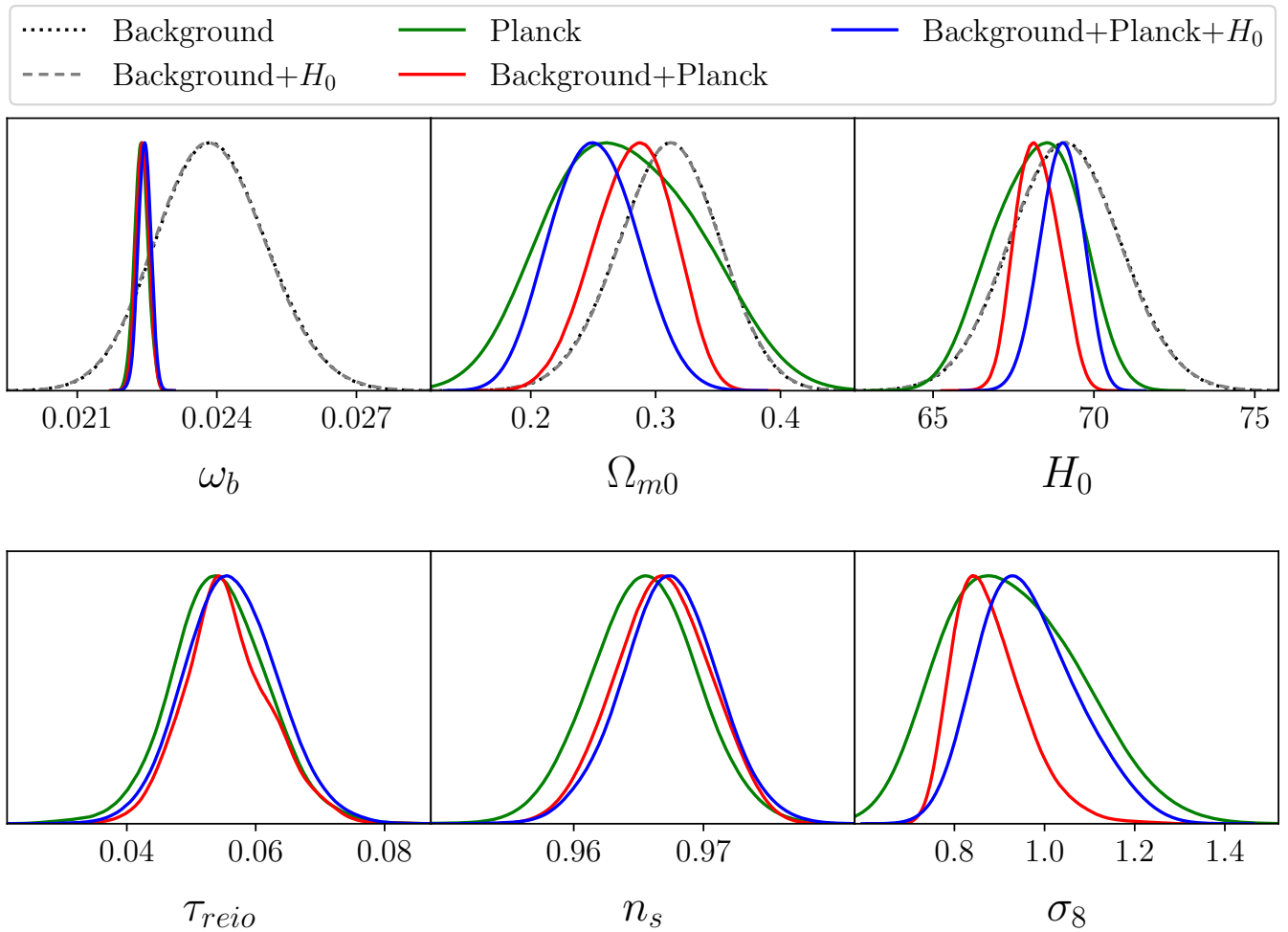


Fig. 9. Posteriors for the free cosmological parameters, considering the analyses without WEC prior, using the datasets: Background, Background+ H_0 , Planck, Background+Planck and Background+Planck+ H_0 .

In the case without the WEC prior, adding the Background and H_0 data to the Planck data seems to alleviate the tension in H_0 , which is related to the positive value of the interaction parameter γ . However, considering the WEC prior shifts the constraints to lower values of H_0 , increasing the tension of the Hubble parameter. On the other hand, when the Background and H_0 data are combined with the Planck data, the constraints on H_0 and σ_8 are reasonably improved. The inclusion of the WEC prior significantly improves the parameter constraints, showing a preference for drastically lower values of σ_8 , which alleviates the σ_8 tension between the results from the CMB data (Planck 2018) [32] and the weak gravitational lensing data (KiDS-1000) [62].

In the case without the WEC prior, all datasets show weak constraints on the parameters γ and Ω_{m0} , which improve when the Background and H_0 data are combined with the Planck data.

Our results show an anticorrelation between γ and Ω_{m0} . The inclusion of the WEC prior significantly improves the parameter constraints, resulting in higher values of Ω_{m0} and lower values of σ_8 , which combined lead

to a lower value of S_8 , that is included between the values predicted by Planck 2018 [32], and the values predicted by the cosmic shear surveys [62,63,64]. In any case, our analysis exhibits that the model's predictions are consistent with the current estimates of σ_8 and S_8 within 2σ C.L. regions with the Planck 2018 results.

Data Availability Statement

All data used are already publicly available and properly cited in this paper.

Acknowledgement

JSL acknowledges financial support from the Coordenação de Aperfeiçoamento de Pessoal de Nível Superior - Brasil (CAPES) - Finance Code 001. RvM is supported by Fundação de Amparo à Pesquisa do Estado da Bahia (FAPESB) grant TO APP0039/2023. LC acknowledges CNPq for the partial support. We acknowledge the use of CLASS, MontePython and GetDist codes.

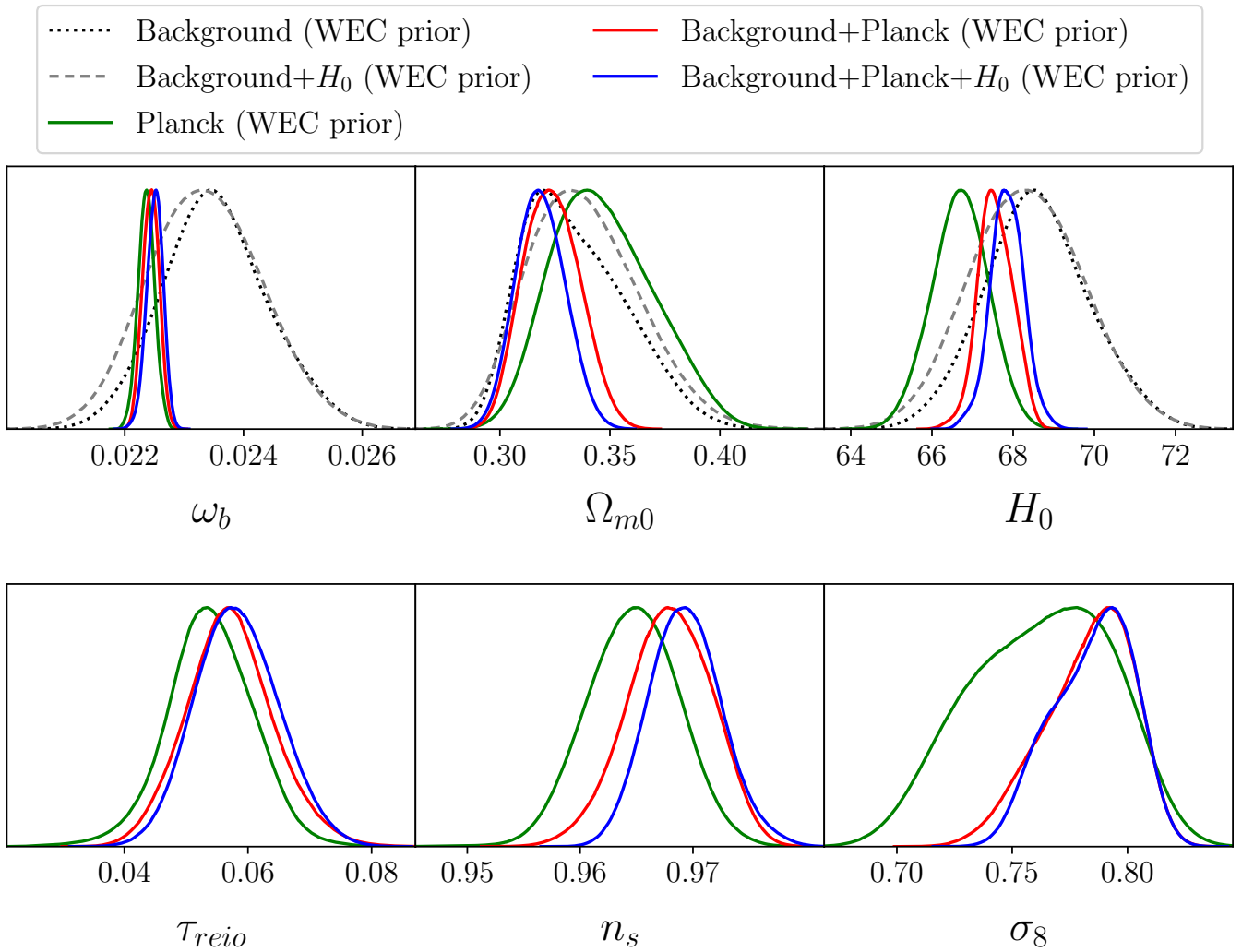


Fig. 10. Posteriors for the free cosmological parameters, considering the analyses with WEC prior, using the datasets: Background, Background+ H_0 , Planck, Background+Planck and Background+Planck+ H_0 .

References

1. Adam G. Riess, Alexei V. Filippenko, Peter Challis, et al. Observational evidence from supernovae for an accelerating universe and a cosmological constant. *The Astronomical Journal*, 116(3):1009–1038, sep 1998.
2. S. Perlmutter, G. Aldering, M. Della Valle, et al. Discovery of a supernova explosion at half the age of the universe. *Nature*, 391(6662):51–54, January 1998.
3. S. Perlmutter, G. Aldering, G. Goldhaber, et al. Measurements of ω and λ from 42 high-redshift supernovae. *The Astrophysical Journal*, 517(2):565–586, jun 1999.
4. J. A. S. Lima. Alternative dark energy models: an overview. *Brazilian Journal of Physics*, 34:194 – 200, 03 2004.
5. George F R Ellis, Henk van Elst, Jeff Murugan, and Jean-Philippe Uzan. On the trace-free einstein equations as a viable alternative to general relativity. *Classical and Quantum Gravity*, 28(22):225007, oct 2011.
6. M. Sami. A primer on problems and prospects of dark energy. *arXiv e-prints*, page arXiv:0904.3445, apr 2009.
7. H. E. S. Velten, R. F. vom Marttens, and W. Zimdahl. Aspects of the cosmological “coincidence problem”. *The European Physical Journal C*, 74(1):3160, 2014.
8. Steven Weinberg. The cosmological constant problem. *Rev. Mod. Phys.*, 61:1–23, Jan 1989.
9. Ivaylo Zlatev, Limin Wang, and Paul J. Steinhardt. Quintessence, cosmic coincidence, and the cosmological constant. *Phys. Rev. Lett.*, 82:896–899, Feb 1999.
10. Rodrigo von Marttens, L. Casarini, D.F. Mota, and W. Zimdahl. Cosmological constraints on parametrized interacting dark energy. *Physics of the Dark Universe*, 23:100248, 2019. arXiv:1807.11380 [astro-ph.CO].
11. P. J. E. Peebles and Bharat Ratra. The cosmological constant and dark energy. *Rev. Mod. Phys.*, 75:559–606, Apr 2003.
12. S. Q. Hou, J. J. He, A. Parikh, et al. Non-extensive statistics to the cosmological lithium problem. *The Astrophysical Journal*, 834(2):165, jan 2017.
13. Salvatore Capozziello, Giuseppe Sarracino, and Giulia De Somma. A critical discussion on the h_0 tension. *Universe*, 10(3), 2024.

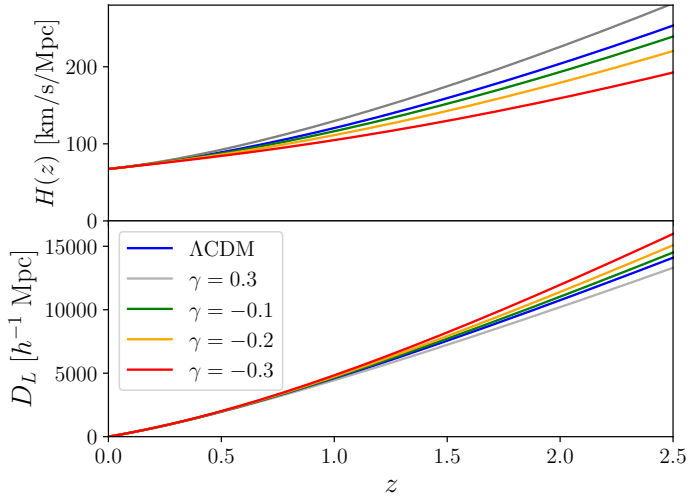


Fig. 11. The top panel shows the expansion rate $H(z)$ as a function of redshift z for different values of γ , while the bottom panel displays the luminosity distance D_L for the same γ values.

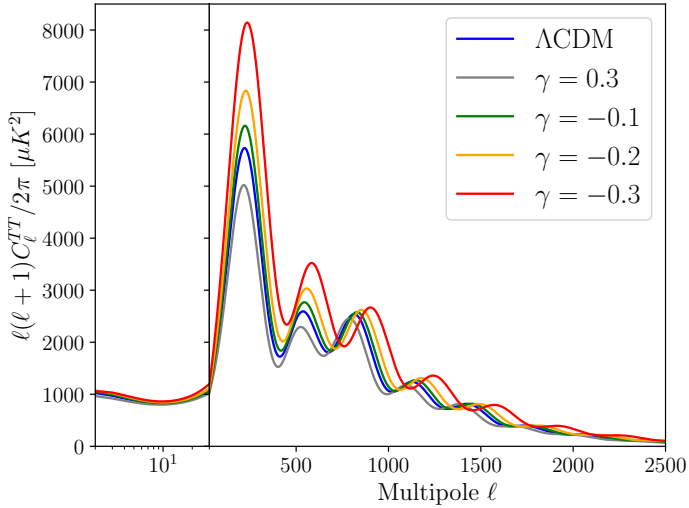


Fig. 12. CMB temperature power spectra for different values of γ . We used the CLASS code, and for the Λ CDM model, we fixed the parameters $\gamma = 0$, $\omega_x = -1$, $\omega_c = 0.1200$, $\omega_b = 0.02237$, and $h = 0.6736$ [32], respectively.

14. Kazuharu Bamba, Salvatore Capozziello, Shin'ichi Nojiri, and Sergei D. Odintsov. Dark energy cosmology: the equivalent description via different theoretical models and cosmography tests. *Astrophysics and Space Science*, 342(1):155–228, 2012.

15. S. K. J. Pacif. Dark energy models from a parametrization of h : a comprehensive analysis and observational constraints. *The European Physical Journal Plus*, 135(10):792, 2020.

16. R. von Marttens, H. A. Borges, S. Carneiro, J. S. Alcaniz, and W. Zimdahl. Unphysical properties in a class of interacting dark energy models. *The European Physical Journal C*, 80:1110, dec 2020.

17. Rodrigo von Marttens, Dinorah Barbosa, and Jailson Alcaniz. One-parameter dynamical dark-energy from the generalized chaplygin gas. *Journal of Cosmology and As-*

troparticle Physics, 2023(04):052, apr 2023.

18. Eleonora Di Valentino, Alessandro Melchiorri, Olga Mena, and Sunny Vagnozzi. Interacting dark energy in the early 2020s: A promising solution to the H_0 and cosmic shear tensions. *Phys. Dark Univ.*, 30:100666, 2020.

19. Rafael C. Nunes, Sunny Vagnozzi, Suresh Kumar, Eleonora Di Valentino, and Olga Mena. New tests of dark sector interactions from the full-shape galaxy power spectrum. *Phys. Rev. D*, 105:123506, Jun 2022.

20. Suresh Kumar. Remedy of some cosmological tensions via effective phantom-like behavior of interacting vacuum energy. *Physics of the Dark Universe*, 33:100862, 2021.

21. Eleonora Di Valentino, Alessandro Melchiorri, Olga Mena, and Sunny Vagnozzi. Nonminimal dark sector physics and cosmological tensions. *Phys. Rev. D*, 101:063502, Mar 2020.

22. D. Rowland and I. B. Whittingham. Models of interacting dark energy. *Monthly Notices of the Royal Astronomical Society*, 390(4):1719–1726, 10 2008.

23. Keshav Ram Mishra, Shibesh Kumar Jas Pacif, Rajesh Kumar, and Kazuharu Bamba. Cosmological implications of an interacting model of dark matter & dark energy. *Physics of the Dark Universe*, 40:101211, 2023.

24. Adam G. Riess et al. A 2.4% Determination of the Local Value of the Hubble Constant. *Astrophys. J.*, 826(1):56, 2016.

25. Rodrigo von Marttens, Lucas Lombriser, Martin Kunz, Valerio Marra, Luciano Casarini, and Jailson Alcaniz. Dark degeneracy i: Dynamical or interacting dark energy? *Physics of the Dark Universe*, 28:100490, 2020.

26. Rodrigo von Marttens, Javier E. Gonzalez, Jailson Alcaniz, Valerio Marra, and Luciano Casarini. Model-independent reconstruction of dark sector interactions. *Phys. Rev. D*, 104:043515, Aug 2021.

27. Chung-Pei Ma and Edmund Bertschinger. Cosmological perturbation theory in the synchronous and conformal Newtonian gauges. *Astrophys. J.*, 455:7–25, 1995.

28. Elisabetta Majerotto, Jussi Väliiviita, and Roy Maartens. Adiabatic initial conditions for perturbations in interacting dark energy models. *Monthly Notices of the Royal Astronomical Society*, 402(4):2344–2354, 03 2010.

29. Weiqiang Yang, Supriya Pan, and David F. Mota. Novel approach toward the large-scale stable interacting dark-energy models and their astronomical bounds. *Phys. Rev.*, D96(12):123508, 2017.

30. Gabriela Caldera-Cabral, Roy Maartens, and Bjoern Malte Schaefer. The Growth of Structure in Interacting Dark Energy Models. *JCAP*, 0907:027, 2009.

31. Edward W Kolb, Sabino Matarrese, and Antonio Riotto. On cosmic acceleration without dark energy. *New Journal of Physics*, 8(12):322, dec 2006.

32. Planck Collaboration, N. Aghanim, Y. Akrami, M. Ashdown, et al. Planck 2018 results - vi. cosmological parameters. *A&A*, 641:A6, 2020.

33. D. M. Scolnic, D. O. Jones, A. Rest, et al. The complete light-curve sample of spectroscopically confirmed SNe ia from pan-STARRS1 and cosmological constraints from the combined pantheon sample. *The Astrophysical Journal*, 859(2):101, may 2018.

34. M. Betoule, R. Kessler, J. Guy, et al. Improved cosmological constraints from a joint analysis of the sdss-ii and snls supernova samples. *Astronomy and Astrophysics*, 568:A22, 2014.

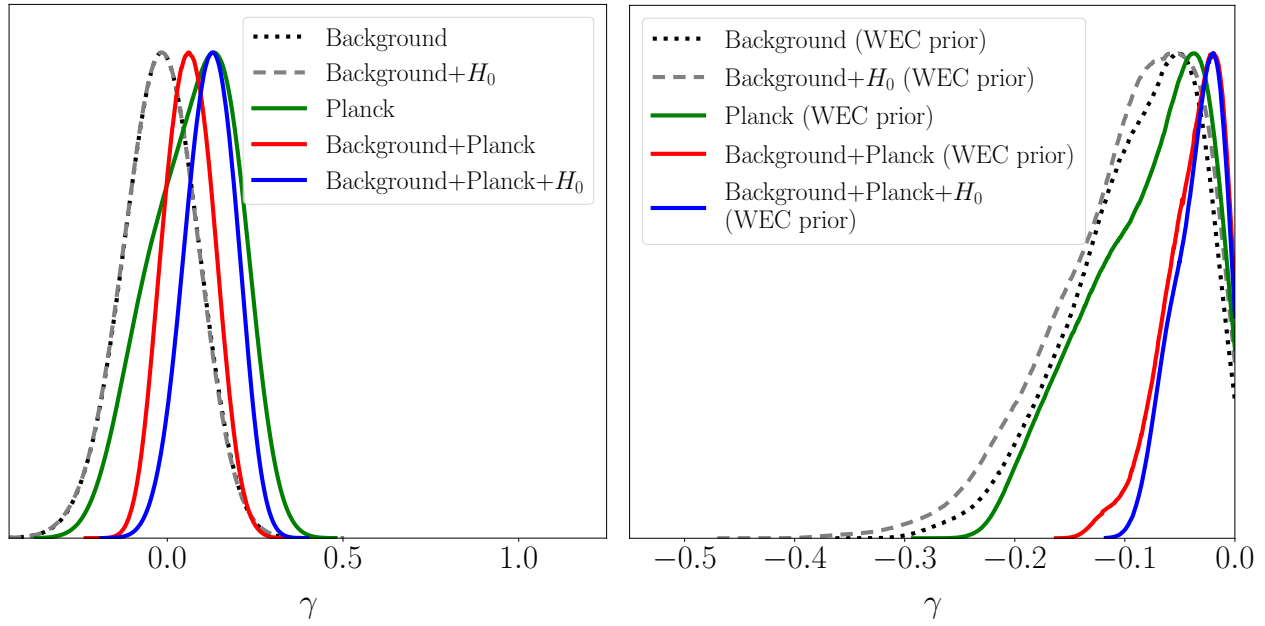


Fig. 13. Posteriors for the interaction parameter γ : without the use of a WEC prior (left panel) and with the application of the WEC prior (right panel).

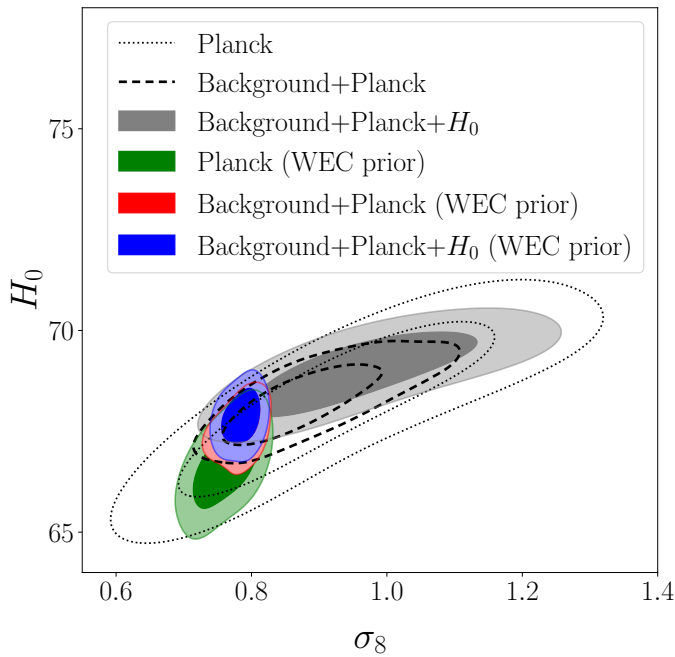


Fig. 14. Plot of the parameter σ_8 versus the Hubble parameter H_0 without the WEC prior and with the WEC prior.

35. Michele Moresco, Lucia Pozzetti, Andrea Cimatti, Raul Jimenez, Claudia Maraston, Licia Verde, Daniel Thomas, Annalisa Citro, Rita Tojeiro, and David Wilkinson. A 6% measurement of the hubble parameter at $z \sim 0.45$: direct evidence of the epoch of cosmic re-acceleration. *Journal of Cosmology and Astroparticle Physics*, 2016(05):014–014, may 2016.

36. Cong Zhang, Han Zhang, Shuo Yuan, Siqi Liu, Tong-Jie Zhang, and Yan-Chun Sun. Four new observational $H(z)$ data from luminous red galaxies in the sloan digital sky survey data release seven. *Research in Astronomy and Astrophysics*, 14(10):1221–1233, sep 2014.

37. Joan Simon, Licia Verde, and Raul Jimenez. Constraints on the redshift dependence of the dark energy potential. *Phys. Rev.*, D71:123001, 2005.

38. M. Moresco et al. Improved constraints on the expansion rate of the Universe up to z 1.1 from the spectroscopic evolution of cosmic chronometers. *JCAP*, 1208:006, 2012.

39. Daniel Stern, Raul Jimenez, Licia Verde, Marc Kamionkowski, and S. Adam Stanford. Cosmic Chronometers: Constraining the Equation of State of Dark Energy. I: $H(z)$ Measurements. *JCAP*, 1002:008, 2010.

40. Michele Moresco. Raising the bar: new constraints on the Hubble parameter with cosmic chronometers at $z \sim 2$. *Monthly Notices of the Royal Astronomical Society, Letters*, 450(1):L16–L20, 04 2015.

41. Bruce A. Bassett and Renée Hlozek. Baryon acoustic oscillations, 2009.

42. Daniel J. Eisenstein, Hee-Jong Seo, and Martin White. On the Robustness of the Acoustic Scale in the Low-Redshift Clustering of Matter. *APJ*, 664(2):660–674, aug 2007.

43. Andoni Aizpuru, Rubén Arjona, and Savvas Nesseris. Machine learning improved fits of the sound horizon at the baryon drag epoch. *Phys. Rev. D*, 104:043521, Aug 2021.

44. Daniel J. Eisenstein, Idit Zehavi, David W. Hogg, et al. Detection of the baryon acoustic peak in the large-scale correlation function of SDSS luminous red galaxies. *The Astrophysical Journal*, 633(2):560–574, nov 2005.

45. Balakrishna S. Haridasu, Vladimir V. Luković, and Nicola Vittorio. Isotropic vs. anisotropic components of bao data: a tool for model selection. *Journal of Cosmology and Astroparticle Physics*, 2018(05):033, may 2018.

46. Lauren Anderson et al. The clustering of galaxies in the SDSS-III Baryon Oscillation Spectroscopic Survey: baryon

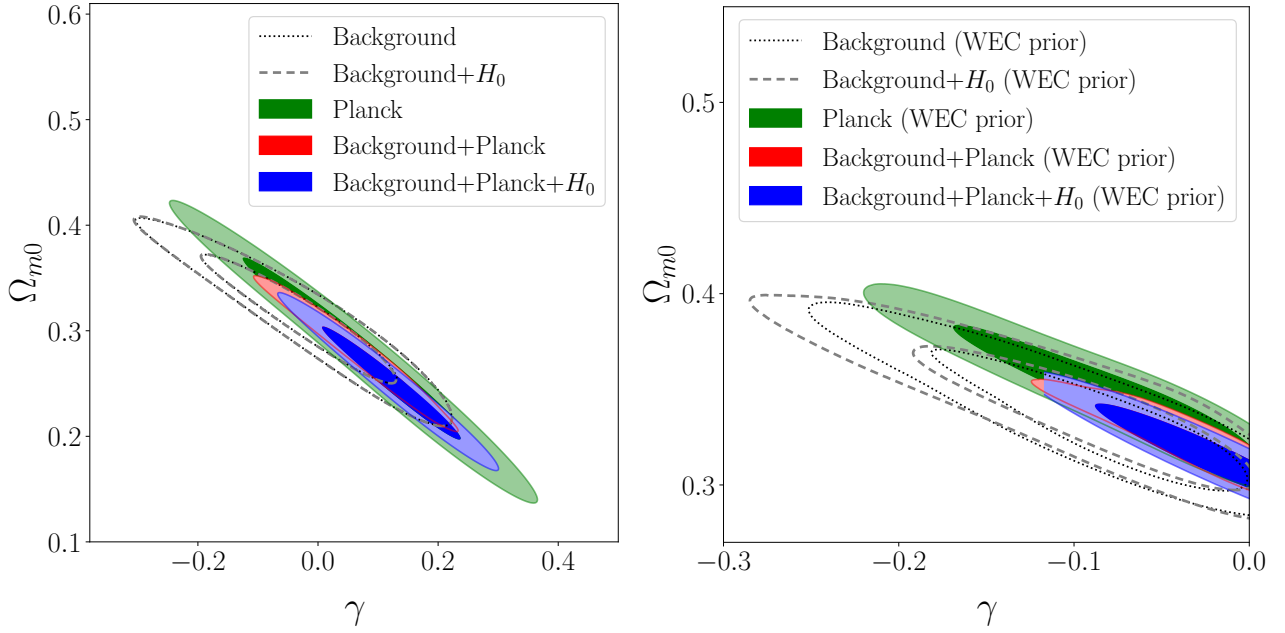


Fig. 15. Plot of the interaction parameter γ versus the matter density parameter Ω_{m0} without the WEC prior (left panel) and with the WEC prior (right panel).

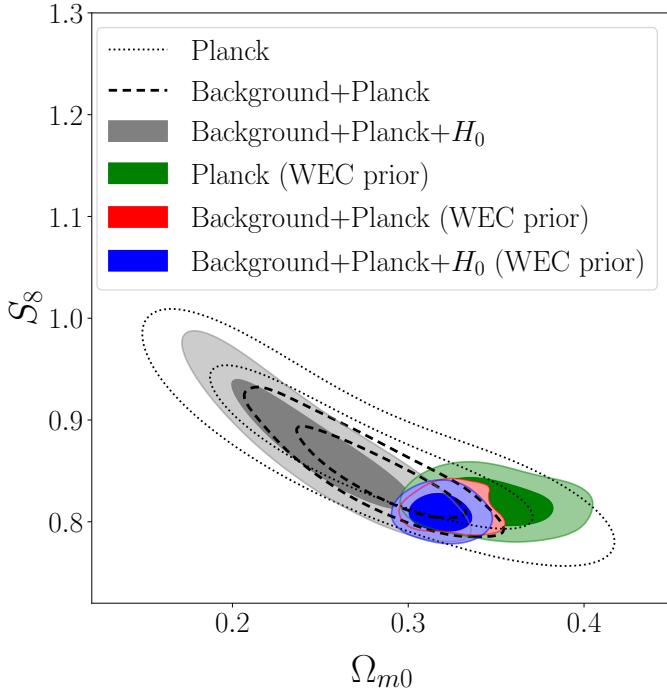


Fig. 16. Plot of the matter density parameter Ω_{m0} versus the parameter S_8 without the WEC prior and with the WEC prior.

acoustic oscillations in the Data Releases 10 and 11 Galaxy samples. *Mon. Not. Roy. Astron. Soc.*, 441(1):24–62, 2014.

47. Ashley J. Ross, Lado Samushia, Cullan Howlett, Will J. Percival, Angela Burden, and Marc Manera. The clustering of the SDSS DR7 main Galaxy sample – I. A 4 per cent distance measure at $z = 0.15$. *Mon. Not. Roy. Astron. Soc.*, 449(1):835–847, 2015.

48. Andreu Font-Ribera, David Kirkby, Nicolas Busca, et al. Quasar-lyman α forest cross-correlation from boss: Baryon acoustic oscillations. *Journal of Cosmology and Astroparticle Physics*, 2014(05):027, may 2014.
49. Planck Collaboration, Aghanim, N., Akrami, Y., Ashdown, M., et al. Planck 2018 results - v. cmb power spectra and likelihoods. *A&A*, 641:A5, 2020.
50. Thejs Brinckmann and Julien Lesgourgues. Montepython 3: Boosted mcmc sampler and other features. *Physics of the Dark Universe*, 24:100260, 2019.
51. Benjamin Audren, Julien Lesgourgues, Karim Benabed, and Simon Prunet. Conservative constraints on early cosmology with monte python. *Journal of Cosmology and Astroparticle Physics*, 2013(02):001, feb 2013.
52. Diego Blas, Julien Lesgourgues, and Thomas Tram. The cosmic linear anisotropy solving system (CLASS). part II: Approximation schemes. *Journal of Cosmology and Astroparticle Physics*, 2011(07):034–034, jul 2011.
53. Nicholas Metropolis, Arianna W. Rosenbluth, Marshall N. Rosenbluth, Augusta H. Teller, and Edward Teller. Equation of state calculations by fast computing machines. *The Journal of Chemical Physics*, 21(6):1087–1092, 1953.
54. W. K. Hastings. Monte Carlo sampling methods using Markov chains and their applications. *Biometrika*, 57(1):97–109, 04 1970.
55. Dootika Vats and Christina Knudson. Revisiting the Gelman-Rubin Diagnostic. *arXiv e-prints*, page arXiv:1812.09384, December 2018.
56. Andrew Gelman and Donald B. Rubin. Inference from iterative simulation using multiple sequences. *Statist. Sci.*, 7(4):457–472, 11 1992.
57. Antony Lewis. Getdist: a python package for analysing monte carlo samples, 2019.
58. Antony Lewis. GetDist: Monte Carlo sample analyzer. Astrophysics Source Code Library, record ascl:1910.018, October 2019.

59. Wayne Hu and Scott Dodelson. Cosmic microwave background anisotropies. *Annual Review of Astronomy and Astrophysics*, 40(Volume 40, 2002):171–216, 2002.
60. David Wands, Oliver F. Piattella, and Luciano Casarini. Physics of the cosmic microwave background radiation. In Júlio C. Fabris, Oliver F. Piattella, Davi C. Rodrigues, Hermano E.S. Velten, and Winfried Zimdahl, editors, *The Cosmic Microwave Background*, pages 3–39, Cham, 2016. Springer International Publishing.
61. R.F. vom Marttens, L. Casarini, W. Zimdahl, W.S. Hipólito-Ricaldi, and D.F. Mota. Does a generalized chaplygin gas correctly describe the cosmological dark sector? *Physics of the Dark Universe*, 15:114–124, 2017.
62. Heymans, Catherine, Tröster, Tilman, Asgari, Marika, et al. Kids-1000 cosmology: Multi-probe weak gravitational lensing and spectroscopic galaxy clustering constraints. *A&A*, 646:A140, 2021.
63. Shahab Joudaki, Alexander Mead, Chris Blake, et al. KiDS-450: testing extensions to the standard cosmological model. *Monthly Notices of the Royal Astronomical Society*, 471(2):1259–1279, 04 2017.
64. Shahab Joudaki, Chris Blake, Andrew Johnson, Alexandra Amon, et al. KiDS-450 + 2dFLenS: Cosmological parameter constraints from weak gravitational lensing tomography and overlapping redshift-space galaxy clustering. *Monthly Notices of the Royal Astronomical Society*, 474(4):4894–4924, 10 2017.
65. M. A. Troxel, N. MacCrann, J. Zuntz, et al. Dark energy survey year 1 results: Cosmological constraints from cosmic shear. *Phys. Rev. D*, 98:043528, Aug 2018.
66. A. Amon, D. Gruen, M. A. Troxel, N. MacCrann, et al. Dark energy survey year 3 results: Cosmology from cosmic shear and robustness to data calibration. *Phys. Rev. D*, 105:023514, Jan 2022.

A Observational Results of the Λ CDM Model

Additionally, we will present a rectangular plot with the results for the Λ CDM model, as shown in Fig. 17 and the plot of posteriors in Fig. 18, along with Tables 4 and 5 displaying the main cosmological parameters within a 1σ C.L. for this model.

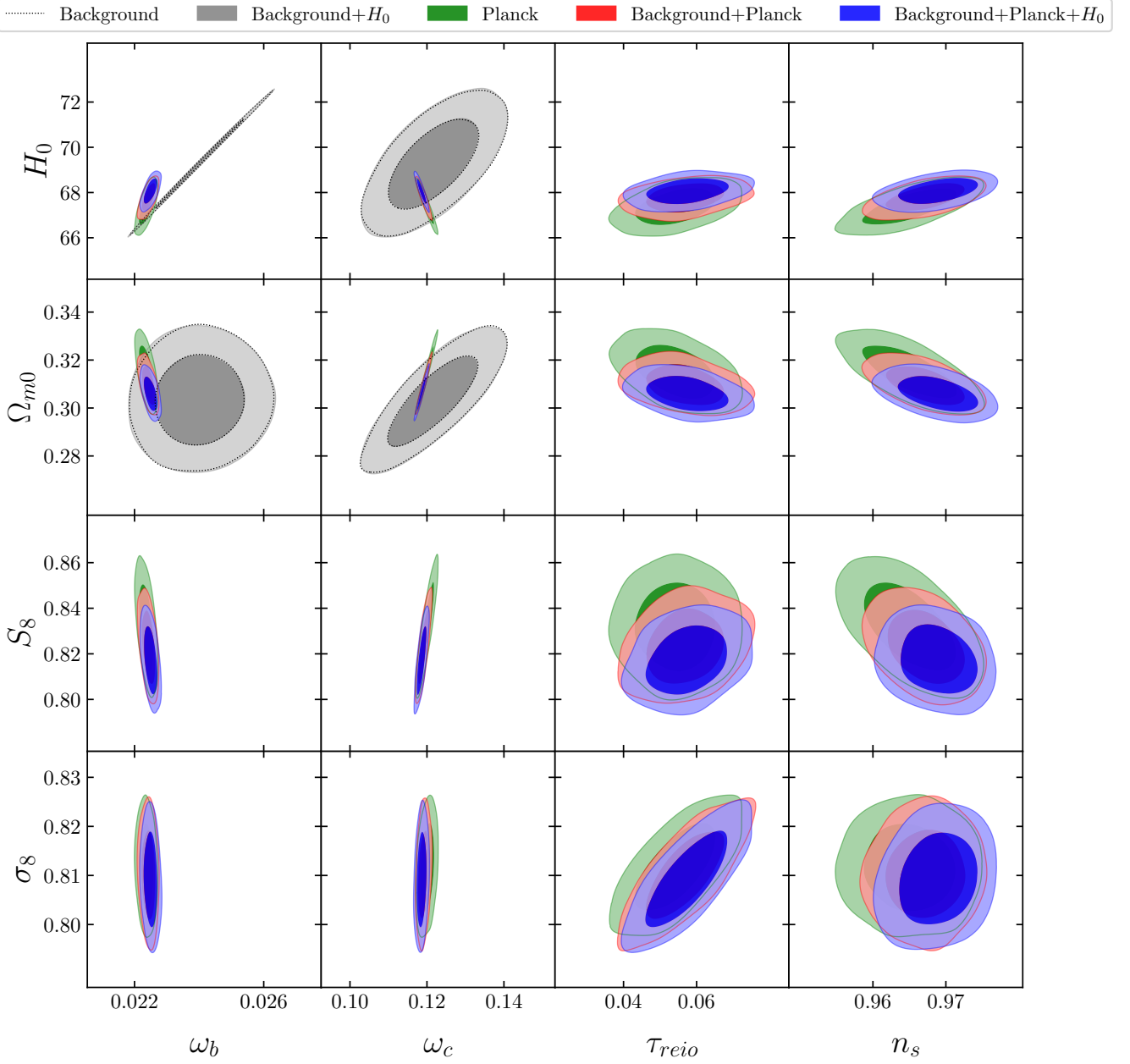


Fig. 17. Rectangular plot with the free cosmological parameters in the Λ CDM model, using the datasets: Background, Background+ H_0 , Planck, Background+Planck and Background+Planck+ H_0 .

Table 4. Results of the statistical analysis of the Λ CDM model at 1σ C.L., using the datasets: Background, and Background+ H_0 .

Parameter	Background	Background+ H_0
ω_c	$0.1218^{+0.0078}_{-0.0078}$	$0.1217^{+0.0077}_{-0.0077}$
H_0	$69.3^{+1.3}_{-1.3}$	$69.3^{+1.3}_{-1.3}$
ω_b	$0.02402^{+0.00091}_{-0.00091}$	$0.02402^{+0.00092}_{-0.00092}$
Ω_{m0}	$0.304^{+0.012}_{-0.012}$	$0.303^{+0.013}_{-0.013}$

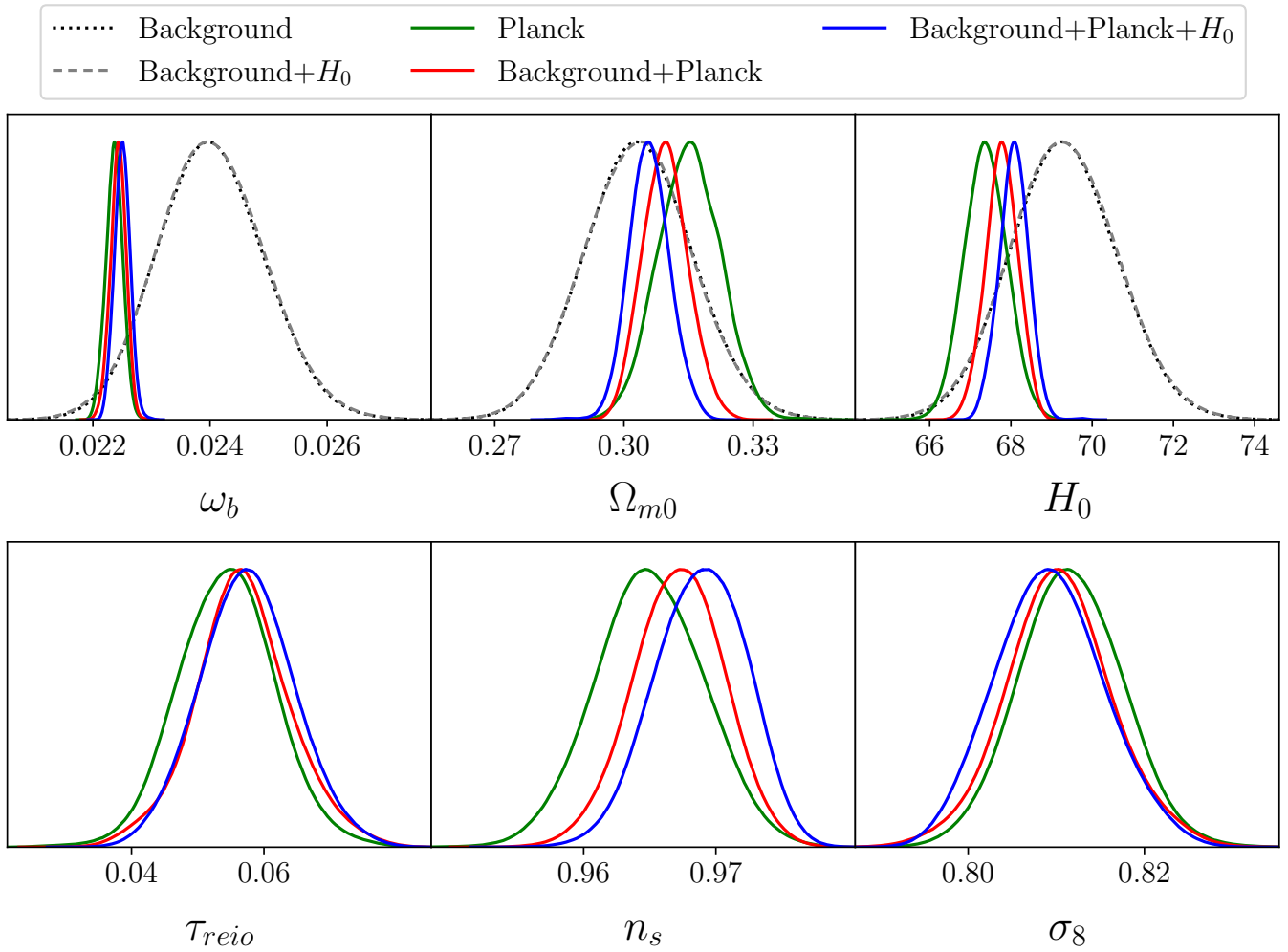


Fig. 18. Posteriors for the free cosmological parameters in the Λ CDM model, using the datasets: Background, Background+ H_0 , Planck, Background+Planck and Background+Planck+ H_0 .

Table 5. Results of the statistical analysis of the Λ CDM model at 1σ C.L., using the datasets: Planck, Planck+Background, and Planck+Background+ H_0 .

Parameter	Planck	Background+Planck	Background+Planck+ H_0
$100\theta_s$	$1.04189^{+0.00029}_{-0.00029}$	$1.04195^{+0.00029}_{-0.00029}$	$1.04207^{+0.00026}_{-0.00026}$
$\ln 10^{10} A_s$	$3.045^{+0.014}_{-0.014}$	$3.048^{+0.014}_{-0.014}$	$3.049^{+0.013}_{-0.016}$
n_s	$0.9650^{+0.0041}_{-0.0041}$	$0.9672^{+0.0035}_{-0.0035}$	$0.96889^{+0.0037}_{-0.0033}$
ω_b	$0.02237^{+0.00014}_{-0.00014}$	$0.02243^{+0.00014}_{-0.00013}$	$0.02250^{+0.00013}_{-0.00013}$
ω_c	$0.1200^{+0.0012}_{-0.0012}$	$0.11913^{+0.00088}_{-0.00088}$	$0.11858^{+0.00079}_{-0.00079}$
τ_{reio}	$0.0544^{+0.0074}_{-0.0074}$	$0.0568^{+0.0073}_{-0.0073}$	$0.0575^{+0.0071}_{-0.0071}$
H_0	$67.38^{+0.53}_{-0.53}$	$67.78^{+0.40}_{-0.40}$	$68.08^{+0.37}_{-0.37}$
Ω_{m0}	$0.3152^{+0.0073}_{-0.0073}$	$0.3096^{+0.0053}_{-0.0053}$	$0.3059^{+0.0048}_{-0.0048}$
σ_8	$0.8116^{+0.0059}_{-0.0059}$	$0.8103^{+0.0061}_{-0.0061}$	$0.8093^{+0.0061}_{-0.0061}$
S_8	$0.832^{+0.013}_{-0.013}$	$0.823^{+0.010}_{-0.010}$	$0.8171^{+0.0093}_{-0.0100}$